

Design of Four-Band Multispectral Imaging System with One Single-Sensor

Bangyong Sun^{1,2}; Nianzeng Yuan¹; Congjun Cao¹; Jon Y. Hardeberg²

1. *Research Centre of Printing and Packaging Engineering, Shaanxi Province of China, Xi'an University of China, Xi'an 710048, China*
2. *Norwegian Colour and Visual Computing Laboratory, Norwegian University of Science and Technology, N-2802 Gjøvik, Norway*

Abstract: In order to acquire multispectral images precisely and quickly, a four-band multispectral capturing system with one imaging sensor is designed and evaluated in this paper. Firstly, four imaging bands are arranged in a 2×2 multispectral filter array (MSFA), and their filter spectral transmittances within the visual wavelength are designed uniformly. Then, the mosaicked four-band image is generated on the single-sensor according to the designed MSFA. In order to recover the mosaicked images, a demosaicking algorithm based on constant hue assumption is employed to highly maintain the image edges. At last, the four-band spectral capturing system is characterized by using the calibration target Macbeth Colorchecker, and a linear relationship between the band values and spectrum are calculated based on polynomial regression method, afterwards the demosaicked four-band pixels can be converted into the multispectral reflectance with that obtained relationship. In the experiment, the four-band multispectral imaging system with the proposed demosaicking algorithm is evaluated, and the experiment result demonstrates the proposed algorithm outperform the other methods in PSNR and RRMS.

Key words: multispectral image; demosaicking algorithm; multispectral filter array (MSFA)

1 INTRODUCTION

Multispectral image is a composition of several monochrome images normally captured with different sensors. Each monochrome image and sensor corresponds to specific wavelength which is usually referred to as a band or channel. Compared to classical RGB images, multispectral images contain much more information in the visible or invisible wavelength. Now multispectral images have been widely used in the area of aerospace, biomedical, agriculture, cultural heritage, and so on, thus it's significant to develop precise and fast multispectral capturing systems.

In the past few decades, many types of multispectral acquisition systems have been developed which normally employ the prism or diffraction grating to split the light and thereby several imaging sensors are installed [1]. As traditional multispectral cameras could not precisely capture the moving objects or reflect disadvantages in the case of product size or cost, new multispectral imaging techniques with filters array and single sensor have been proposed in the recent years. Single-sensor multispectral imaging is actually the extension from the CFA (color filter arrays) to the MSFA (multispectral filter array). Similar to the CFAs involved in most digital cameras, the MSFA is designed for down-sampling which is mainly determined by the amount and the spatial distribution of spectral bands [2-4]. Multispectral capturing system with single-sensor can acquire the spectral images in one shot, and possess the advantage of accurate image registration, low cost and small size. However, because single sensor is applied during multispectral imaging, only one band of spectral information is sampled at each pixel which means the information of other bands is neglected. In order to get the integrated spectral data of each pixel, the lost information of the other bands must be recovered with demosaicking algorithms. Multispectral demosaicking is always a challenging problem because of the sparse sampling, and undesired artifact effects are usually involved in the restored images, such as zipper effect, false color, aliasing, or blurring problems. Besides, several other procedures should be considered during the design of single-sensor multispectral imaging systems, such as

filter design, MSFA tessellation(or mosaicking), spectrum restoration, spectral image processing, etc[5]. The quality of the captured multispectral images highly depends on the precision of these procedures.

The number of bands or the amount of filters in the MSFA largely determines the sampling rate of each pixel. For instance, RGB digital cameras usually apply three filters in a 2×2 Bayer CFA[6-8], and only one third of the color information is sampled on the single sensor which means two thirds of data is lost. In single-sensor multispectral systems, four, five, six, eight, and even more filters have been employed[2, 9-12], thus more color/spectrum data is lost than RGB cameras with Bayer CFA. The much lower sampling rate greatly challenges the design of snapshot multispectral cameras, especially the process of demosaicking and spectrum restoration[2, 9, 13]. In this paper, the basic procedures of a four-band multispectral imaging system are designed and evaluated. Firstly, the visible spectrum from 400nm to 700nm is sampled with four band-pass filters in a 2×2 array, and then a mosaicked multispectral image is projected on the sensor with only 1/4 information is captured. In order to recover the other three bands from the sample data of each pixel, an effective demosaicking algorithm is proposed which well preserves the image edges. At last the spectrum data is restored from the demosaicked four-band image based on several coefficients calculated by spectral characterization.

The remainder of this paper is organized as follows. In **Section 2**, the frame of the multispectral capturing system is described, and diverse multispectral filter arrays are introduced. **Section 3** describes the demosaicking process which interpolates the missing bands along the image edge directions, and the demosaicked image is further corrected by using wavelet transform method. In **section4**, the multispectral imaging system is characterized where a relationship between four-band imaging values and spectral values is generated, and the spectrum of each pixel is estimated from the demosaicked image. In **Section 5**, the designed multispectral imaging system is simulated and evaluated with the metrics of PSNR and spectrum difference RRMS. At last **Section 6** draws the conclusions.

2 WORKFLOW OF SINGLE-SENSOR MULTISPECTRAL IMAGING SYSTEM

2.1 CAPTURING THE MULTISPECTRAL IMAGE WITH SINGLE-SENSOR

Different from the prevalent RGB digital cameras, the single-sensor multispectral capturing system does not export RGB images but the spectral images. Generally, multispectral imaging process can be described as follows[2]. Firstly, the light of an illuminant is reflected from the surface of objects and goes through the camera lens, and then the incident light is separated by different filters in front of the imaging sensor. As one pixel corresponds to only one specific filter, the response of the monochrome sensor is actually a mosaicked image which is heavily dependent on the filter transmittance curves and the MSFA. At the end, the mosaicked image will be demosaicked for spectrum reconstruction. In this section, the multispectral imaging principle on the single-sensor is presented, and various filter transmittance designs and filter arrays are listed.

The multispectral imaging process can be regarded as a linear mapping from the incident light radiance to the sensor responses. When the sensor's spectral response is expressed using a function $L_s(\lambda)$, and the spatial response function is denoted as $h_s(x,y)$ which describes the optical blur and spatial integration at each sensor site, the discrete imaging process can be defined as:

$$S(x, y) = \sum_{\lambda} \sum_{\Delta x, \Delta y} L_s(\lambda) h_s(x - \Delta x, y - \Delta y) r(\Delta x, \Delta y, \lambda) + N_s(x, y) \quad (1)$$

where $S(x, y)$ represents the intensity at spatial location (x, y) , $r(\Delta x, \Delta y, \lambda)$ denotes the incident radiance, and $N_s(x, y)$ stands

for the additive noise which is a result of thermal/quantum effects and quantization. Since the single-sensor is applied, a mosaic indicator for location (x, y) should be defined as:

$$I_S(x, y) = \begin{cases} 1, & \text{if } (x, y) \in \Lambda_S \\ 0, & \text{otherwise} \end{cases} \tag{2}$$

where Λ_S is the set of pixels locations for band S . Finally an N -band single-sensor spectral imaging process raw data is expressed as below:

$$O(x, y) = \sum_{S=S_1, S_2, \dots, S_N} I_S(x, y) S(x, y) \tag{3}$$

2.2 FILTER TRANSMITTANCE DESIGN AND FILTER ARRAYS WITHIN SPECTRAL IMAGING SYSTEMS

Filters control the amount of incident light reaching the sensors by setting specific transmittance of the wavelength. In Bayer’s color filter array, the filter transmittance is designed according to Gaussian distribution which shows great success, and most of the multispectral imaging systems follow this similar filter design principle. If the spectrum λ is sampled from wavelength λ_1 to λ_2 ($\lambda_1 < \lambda < \lambda_2$), the filter transmittance can be expressed as:

$$T(\lambda) = \frac{1}{\sigma\sqrt{2\pi}} e^{-\frac{(\lambda-\mu)^2}{2\sigma^2}} \tag{4}$$

Where μ is the mean or expectation of the transmittance distribution, and σ is the standard deviation of wavelength. By adjusting these two parameters, filters can be designed in the forms of narrow band-pass, wide band-pass, ultrawide band-pass, or the band-reject forms[14, 15]. In the multispectral imaging systems, the wide band-pass filters are usually applied. Because the amount of filters and the corresponding transmittance distribution can be freely set, many forms of filters are designed for multispectral imaging systems. Fig.1(a)~(d) lists the filter designs with four, six, and eight wide band-pass filters.

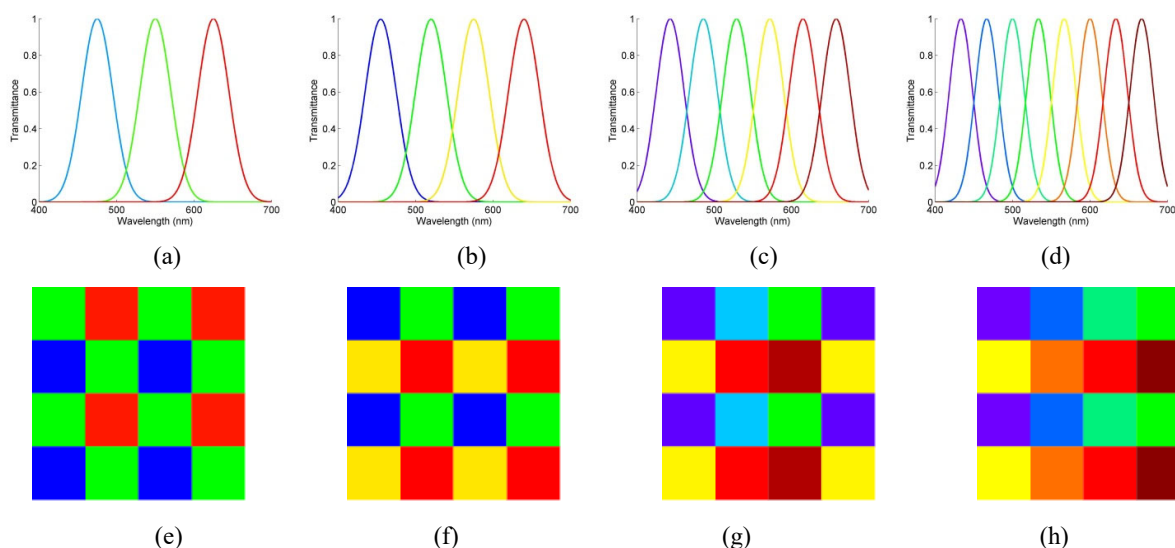


Fig.1 Different filter transmittance curves and arrays within multispectral capture systems: (a)three-band filter design; (b) four-band filter design; (c)six-band filter design; (d)eight-band filter design; (e)Bayer color filter array; (f) 2×2 filter array; (g) 2×3 filter array;

(h) 2×4 filter array.

The number of filters usually determines the quantity of image bands on the monochrome sensor, and the flexibility of those filters’ spatial distribution has great influence on the demosaicking process. An example of the filter array for those filter designs is shown in Fig.1(e)~(h). As mentioned before, the filter arrays are not constant even for the same numbers of bands, for instance, the filter array of an eight-band multispectral imaging system can be designed into several forms. In Fig.2(a), eight filters simply arrange in a 1×8 array, and (b) is the 2×4 array similar to Fig.1(h), (c) is another form of (b), while (d) is a 3×3 array with one copy of band 4. Actually there are still many other different designs for eight-band filter, many factors should be considered to find the optimal spectral filter array solution, especially the spectral sampling rate, demosaicking process, spectrum reconstruction, etc. In this paper, four filters in front of the single-sensor are employed to form a 2×2 array, and we focus on its demosaicking process which is analyzed in Section3.

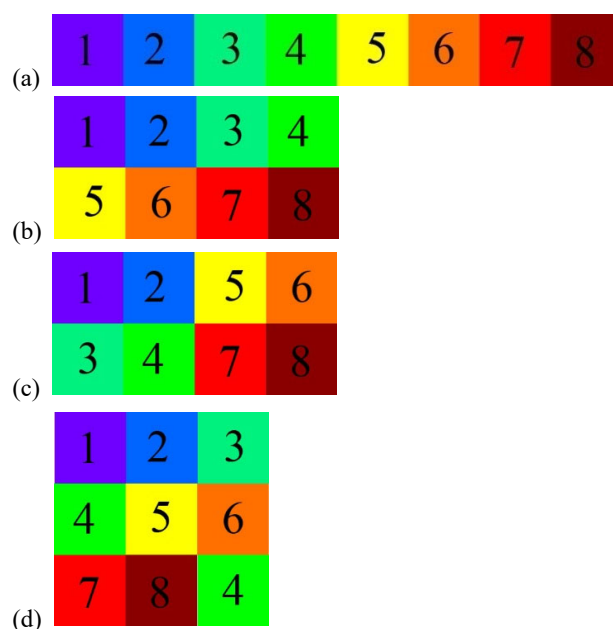


Fig.2 Examples of 8-band filter array

3 MULTISPECTRAL IMAGE DEMOSAICKING FOR THE 2×2 MOSAICKED IMAGES

Within the multispectral imaging process, the multispectral demosaicking for the MSFA is one of the most challenging problems. Large quantities of demosaicking algorithms have been developed for Bayer CFA or MSFA, and several CFA demosaicking methods can be extended to MSFA demosaicking. As shown in Fig.1(a) and (e), three color bands in the Bayer CFA form a 2×2 array which consist of two Green bands, one Red band, and one Blue band. The initial demosaicking algorithms for Bayer CFA recover three bands separately with simple linear interpolations, such as nearest neighbor replacement, bilinear interpolation and bi-cubic interpolation[16-18]. Although those algorithms perform very fast, the demosaicked images usually lost edge details with excessive aliasing or blurring effects. Considering the importance of image edges, the right interpolation direction is computed and applied to several demosaicking algorithms, so that the interpolation is performed along image edges but not across them[19-21]. In addition, there are obvious correlations among different bands for RGB image, many demosaicking models interpolate the image according to constant color ratio or color difference assumption[22-24]. For the multispectral images, the correlation between neighbor bands also maintains.

Now many demosaicking methods have been developed for MSFA, such as bilinear interpolation[25], generic algorithm[10], interpolation with learned weights[11], etc. However, those algorithms' performance is insufficient especially for recovering the image edge details. Thus, in this paper the constant-hue assumption is employed during interpolating the four-band mosaicked image, and the interpolation directions are determined by calculating the gradients of each pixel. Firstly, the image edges are calculated from the mosaicked image, and they are used to define the direction of interpolation with the neighbors. Secondly, the other three bands are recovered from the existed bands for each pixel, by considering the features of filter arrays, image edges and constant-hue features. Thirdly, the wavelet transformation is applied to separate the image into low frequency and high frequency components, and the high frequency images are modified using the luminance information. At last, two metrics are used to evaluate the demosaicking algorithm, one is the modified peak signal-to-noise ratio(PSNR) for the four-band images, and another is the reflectance root mean square (RRMS) which calculates the spectrum errors of the original and reconstructed reflectance values.

3.1 DETERMINING THE INTERPOLATION DIRECTIONS ALONG THE IMAGE EDGES

Some demosaicking algorithms perform well and run quickly in smooth image regions, such as nearest neighbor replication, bilinear interpolation, bi-cubic interpolation, and so on. However, the demosaiced images frequently lose edge details in the texture or structure areas. Edge-detected interpolations can solve those problems by allocating the interpolation directions along the image edges. There are many potential directions involved in the image edges, while the horizontal and vertical directions are mostly utilized for the consideration of the computational efficiency, and sometimes even the diagonal direction is used. In the paper only the horizontal as well as vertical directions are considered.

The gradients are often applied to define the edge directions. Many forms of gradients can be defined according to the spectral filter array, and the simplest gradient-based interpolation with four neighbors is expressed as below.

$$\begin{cases} \Delta H_{i,j} = |I_{i,j-1} - I_{i,j+1}| \\ \Delta V_{i,j} = |I_{i-1,j} - I_{i+1,j}| \end{cases} \quad (5)$$

where $\Delta H_{i,j}$ is the horizontal gradient for position (i, j) , and $\Delta V_{i,j}$ represents the vertical gradient. In most cases, the demosaicking interpolation is performed along the smaller-gradient directions. That is to say, if $\Delta H_{i,j} > \Delta V_{i,j}$, $I_{i,j} = (I_{i-1,j} - I_{i+1,j})/2$, otherwise $I_{i,j} = (I_{i,j-1} - I_{i,j+1})/2$. In reference[26], another expression of gradient is developed for large regions during Bayer CFA demosaicking as below.

$$\begin{cases} \Delta H_{i,j} = |I_{i,j-2} + I_{i,j+2} - 2I_{i,j}| \\ \Delta V_{i,j} = |I_{i-2,j} + I_{i+2,j} - 2I_{i,j}| \end{cases} \quad (6)$$

In this paper four bands of X, Y, Z, W form a 2×2 filter array as shown in Fig.3, and the gradients of the image edges are determined by considering the structure of filter array.

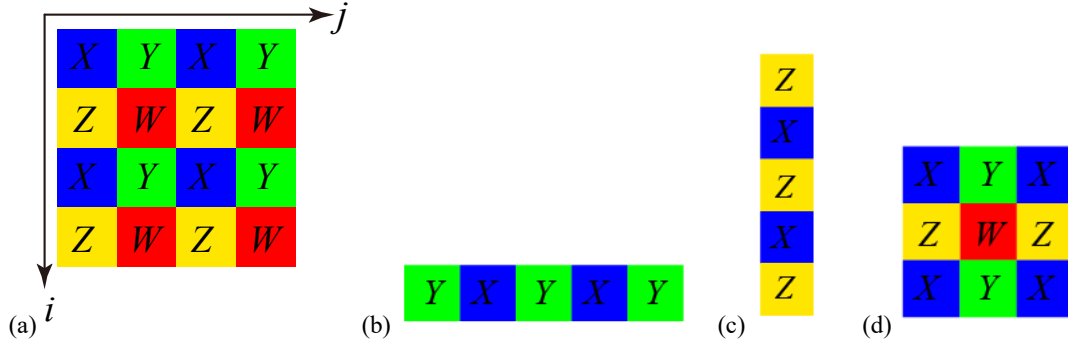


Fig.3 Filter array with four bands: (a) the 2×2 filter array for the four bands; (b) interpolate Y position in horizontal direction; (c) interpolate Z position in vertical direction; (d) interpolate Z position

3.2 INTERPOLATING THE MISSING POSITIONS

As shown in Fig.3, there are one given and three unknown band values for each position. Take the demosaicking process on X band for example, for the 2×2 array the missing X band values in position Y, Z, W are required to be interpolated.

It is relatively simple to recover the X band values in position Y and Z , since there are two nearby X band samples. As shown in Fig.3(b), the Y position can be interpolated along horizontal direction with two X neighbors on both sides. In order to reduce the aliasing effect, the sampled band values of Y are employed based on constant hue assumption which means the hue of an object is constant even for different bands. The hue is sometimes formulated as the color differences or logarithm of color ratios for RGB images, and utilization of constant hue assumption effectively prevent abrupt changes in color intensities. For the four-band mosaic image in this paper, a FIR filter with three coefficients $[0.5 \ 1 \ 0.5]$ and another FIR filter with five coefficients $[-0.25 \ 0 \ 0.5 \ 0 \ -0.25]$ are used during interpolating the middle point as described in reference[27]. So if position (i, j) is a Y position, its X band value can be expressed as:

$$X_{i,j} = \frac{1}{2}(X_{i,j-1} + X_{i,j+1}) + \frac{1}{4}(2Y_{i,j} - Y_{i,j-2} - Y_{i,j+2}) \quad (7)$$

Similarly, if (i, j) is a Z position, its X band values can be estimated by vertical interpolation:

$$X_{i,j} = \frac{1}{2}(X_{i-1,j} + X_{i+1,j}) + \frac{1}{4}(2Z_{i,j} - Z_{i-2,j} - Z_{i+2,j}) \quad (8)$$

At last, the X band value of W position should be interpolated. Because no close X neighbors locate around W position, the new generated X values in Y and Z positions are utilized. As shown in fig.3(d), there are four X neighbors around position W , and the X band values can be interpolated in horizontal or vertical direction. In order to reduce aliasing effect caused by the simple averaging filter, the interpolation is carried out along the image edge directions. The second-order gradients developed by Hamilton and Adams[26] successfully represent the edge directions, so the gradients for position $W(i, j)$ are expressed as:

$$\begin{cases} \Delta H_{i,j} = |X_{i,j-1} - X_{i,j+1}| + |2W_{i,j} - W_{i,j-2} - W_{i,j+2}| \\ \Delta V_{i,j} = |X_{i-1,j} - X_{i+1,j}| + |2W_{i,j} - W_{i-2,j} - W_{i+2,j}| \end{cases} \quad (9)$$

Finally the estimated X band value for W position is determined with the gradient as below.

$$\begin{cases} X_{i,j} = \frac{X_{i-1,j} + X_{i+1,j}}{2} + \frac{2W_{i,j} - W_{i-2,j} - W_{i+2,j}}{4} & \text{if } \Delta H_{i,j} > \Delta V_{i,j} \\ X_{i,j} = \frac{X_{i,j-1} + X_{i,j+1}}{2} + \frac{2W_{i,j} - W_{i,j-2} - W_{i,j+2}}{4} & \text{else} \end{cases} \quad (10)$$

According to Eq.7~10, the unsampled X band values of three positions Y, Z, W within the 2×2 array are interpolated along the lower gradient directions. Similarly, the other band values can be recovered with that method above.

3.3 MODIFY THE HIGH FREQUENCY IMAGE IN WAVELET DOMAIN

Similar to RGB color images, the four-band multispectral image can be separated into luminance and chrominance components. According to the description of imaging process in reference[28,29], the four-band MSFA mosaic data can be written as:

$$O(x, y) = \sum_{S=X,Y,Z,W} m_S(x, y)S(x, y) \quad (11)$$

where $m_S(x, y)$, ($S=X, Y, Z, W$) are the modulation functions at position (x, y) [16]:

$$\begin{cases} m_X(x, y) = (1 + \cos(\pi x)(1 + \cos(\pi y)))/4 \\ m_Y(x, y) = (1 - \cos(\pi x)(1 + \cos(\pi y)))/4 \\ m_Z(x, y) = (1 + \cos(\pi x)(1 - \cos(\pi y)))/4 \\ m_W(x, y) = (1 - \cos(\pi x)(1 - \cos(\pi y)))/4 \end{cases} \quad (12)$$

Based on Eq.11 and Eq.12, the single-sensor image data can be separated into two parts:

$$\begin{aligned} O(x, y) &= \frac{1}{4}(X(x, y) + Y(x, y) + Z(x, y) + W(x, y)) + \frac{1}{4}(X - W)(\cos(\pi x) + \cos(\pi y)) \\ &\quad + \frac{1}{4}(Z - Y)(\cos(\pi x) - \cos(\pi y)) + \frac{1}{4}(X - Y - Z + W) \cos(\pi x) \cos(\pi y) \\ &= \frac{1}{4}(X(x, y) + Y(x, y) + Z(x, y) + W(x, y)) + \sum_{S=X,Y,Z,W} \tilde{m}_S(x, y)S(x, y) \end{aligned} \quad (13)$$

The first term of Eq.13 represents the luminance component and the rest with modulation functions can be seen as chrominance term. The luminance is usually estimated by low-pass filtering, and the chrominance can be estimated by high-pass filtering. Because correlations exist in different bands of spectral image, the image edges within the synthetic luminance component usually well match with four separated bands. In this paper, all the bands of the spectral image are firstly transformed from spatial domain to wavelet domain, and then four separated bands' high frequency components are substituted by the luminance band. The modified image obviously enhances the correlations among different bands and presents fine image edges visually.

From Section 3.2, the demosaicked image consists of four bands of full resolution images, while for each pixel's four band values, only one comes from the initial raw data and the other three are interpolated. When the interpolated band values are optimized, the spectral image will be enhanced. Because wavelet transform has an advantage of processing images in different resolutions, it is applied to separate each image band into four different frequency components. If the decomposition of one band is expressed as $\{LL, LH, HL, HH\}$ in frequency domain, the high frequency information mainly

exists in the set of $\{LH, HL, HH\}$, and they basically represent the edges of image. Since inter-band correlation is involved in the high-frequency, the high frequency coefficients are modified to refine the demosaicked image. The decompositions of four spectral image bands combined with the synthetic luminance band are processed with discrete wavelet transform as below.

$$\begin{cases} \{L_{LL}, L_{LH}, L_{HL}, L_{HH}\} = DWT2(L_{image}) \\ \{X_{LL}, X_{LH}, X_{HL}, X_{HH}\} = DWT2(X_{image}) \\ \{Y_{LL}, Y_{LH}, Y_{HL}, Y_{HH}\} = DWT2(Y_{image}) \\ \{Z_{LL}, Z_{LH}, Z_{HL}, Z_{HH}\} = DWT2(Z_{image}) \\ \{W_{LL}, W_{LH}, W_{HL}, W_{HH}\} = DWT2(W_{image}) \end{cases} \quad (14)$$

Where DWT is the discrete wavelet transform, i_{image} ($i=L, X, Y, Z, W$) represent the luminance and other four spectral image bands. Because the high frequency component of those image bands are highly correlated and have constant variation along the edges[30], four bands' high frequency component can be updated based on this correlation. One common method is to correct them with the luminance band. Driesen and Scheunders[31] proposed two merging rules, in this paper the replacement rule is used, so the high frequency coefficients modification is described as below.

$$\begin{cases} X_i = L_i \\ Y_i = L_i \\ Z_i = L_i \\ W_i = L_i \end{cases} \quad (15)$$

where the subscript $i = LH, HL, HH$ represent the replaced band component for wavelet domain. Finally the inverse wavelet transform is applied to convert the frequency image to spatial domain:

$$\begin{cases} X_{image} = iDWT2(X_{LL}, L_{LH}, L_{HL}, L_{HH}) \\ Y_{image} = iDWT2(Y_{LL}, L_{LH}, L_{HL}, L_{HH}) \\ Z_{image} = iDWT2(Z_{LL}, L_{LH}, L_{HL}, L_{HH}) \\ W_{image} = iDWT2(W_{LL}, L_{LH}, L_{HL}, L_{HH}) \end{cases} \quad (16)$$

where the $iDWT2$ is the inverse wavelet transform.

In fact, some pixel values maybe changed abruptly as the result of wavelet coefficients replacement, so further refinement is usually need after the inverse wavelet transform. In this paper the DWT processed image is further compared with the original demosaicked image, and the band values will be converted into their original values when large difference occurred. Finally, those four recovered bands are combined to form the four-band multispectral image.

3.4 METRICS FOR EVALUATING DEMOSAICKING METHODS

In order to evaluate the demosaicking algorithm, the $PSNR$ metric is firstly employed to compare the original and reconstructed spectral images. For each band of the image, the $PSNR$ is defined as:

$$PSNR = 10 \log_{10} \left(\frac{255^2 H * W}{\sum_{i=1}^H \sum_{j=1}^W (I_o^k(i, j) - I_d^k(i, j))^2} \right) \quad (17)$$

Where H and W represent the height and width of the image, I_o^k and I_d^k are the original and demosaicked images for band K . It should be noted that the band values must be normalized to 0~255 before $PSNR$ calculation. Similar to reference[32], a modified $PSNR$ expression $M-PSNR$ for multispectral image is utilized to evaluate the demosaicking method for the four-

band multispectral image.

$$\begin{cases} M_PSNR = 10\log_{10}\left(\frac{255^2}{MMSE}\right) \\ MMSE = \frac{1}{4H * W} \sum_{k=X,Y,Z,W} \sum_{i=1}^H \sum_{j=1}^W (I_o^k(i,j) - I_d^k(i,j))^2 \end{cases} \quad (18)$$

In addition, as the final output of the multispectral imaging system is the spectrum data of each pixel, the reflectance root mean square (RRMS) error is employed to evaluate the imaging system[33], which is the difference of the original and reconstructed reflectance data expressed as below.

$$RRMS = \frac{1}{H * W} \sum_{i=1}^H \sum_{j=1}^W \sqrt{\frac{\sum_{\lambda} (R_{i,j}(\lambda) - \hat{R}_{i,j}(\lambda))^2}{N}} \quad (19)$$

where $R(\lambda)$ and $\hat{R}(\lambda)$ are the original and estimated reflectance values respectively, and they are scaled to 0~1, while N is the sampled dimensionality of reflectance.

4 SPECTRUM RECONSTRUCTIONS FROM DEMOSAICKED IMAGE

According to the multispectral imaging workflow, the demosaicked image should be finally converted into the original spectrum values. The conversion from multi-band image to spectrum is dependent on a linear relationship which is frequently estimated by using polynomial regression and least square method.

Polynomial regression is a form of linear regression in which the relationship between the independent variable x and the dependent variable y is modeled as an n^{th} degree polynomial. Meanwhile polynomial regression fits a nonlinear relationship between the value of x and the corresponding conditional mean of y values denoted $E(y|x)$, and also has been applied to describe nonlinear phenomena[34]. The multispectral imaging process from spectrum to sensor response can be seen as a liner projection, thus when the reflectance spectrum is sampled as $y_1, y_2 \dots y_n$ and the band values are $x_1, x_2 \dots x_m$, the relation between these two variables can be described as:

$$y_i = \beta_{i0} + \beta_{i1}x_1 + \beta_{i2}x_2 + \dots + \beta_{iM}x_M \quad (20)$$

where i denotes the sequence of discrete reflectance spectrum, so if the spectrum is sampled from 400nm to 700nm with 10nm interval, $i=0, 1, 2, \dots, 30$. The coefficients $\beta_{i0}, \beta_{i1}, \dots, \beta_{iM}$ are the undetermined coefficients for i^{th} spectrum.

In this paper, the color calibration target Macbeth ColorChecker is used to characterize the imaging system. For those 24 groups of color samples, the simulation of spectrum and sensor response is represented in the matrix:

$$Y = X\beta \quad (21)$$

where Y is the 24 color patches' discrete reflectance values from λ_1 to λ_2 , X is the matrix of sensor response. If b_0, b_1, \dots, b_M are the estimated values by least squares methods for parameter β , the regression equation can be expressed as:

$$\hat{y} = b_0 + b_1x_1 + \dots + b_Mx_M \quad (22)$$

From the principle of least squares, the coefficients of b_0, b_1, \dots, b_M should obtain the minimal residuals square sum for

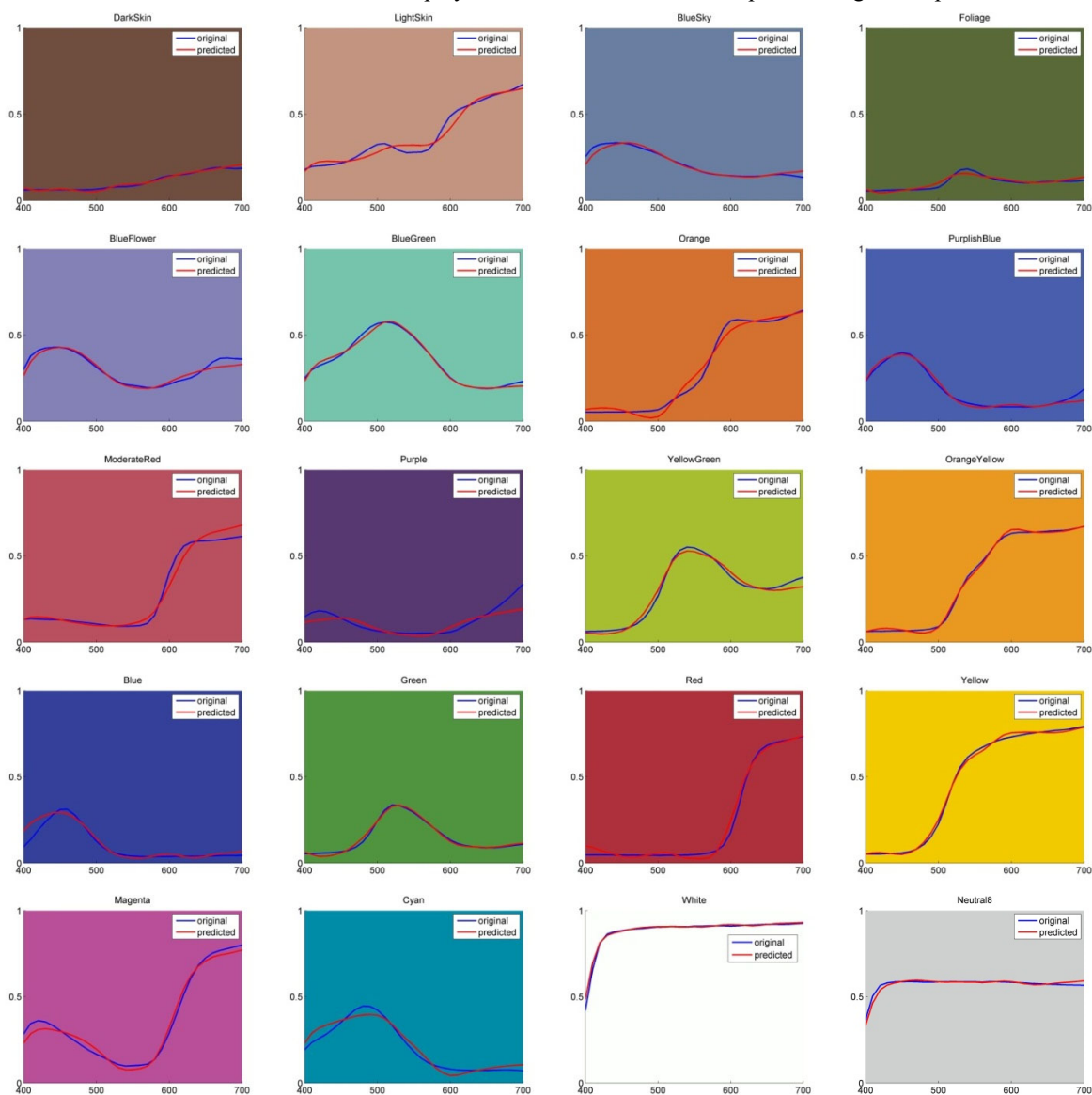
all the measured value y_t and regression value \hat{y}_t :

$$Q = \sum_{t=1}^N (y_t - \hat{y}_t)^2 \tag{23}$$

Finally, the coefficients b can be resolved as below:

$$b = (X^T X)^{-1} X^T Y \tag{24}$$

By using the coefficients above, the spectral values of ColorChecker’s 24 patches are reconstructed and compared with the original values. The comparison is shown in Fig.4 and demonstrates that two groups of spectrum match well, so the coefficients estimated in this section can be employed to reconstruction the multispectral images in experiment of Section5.



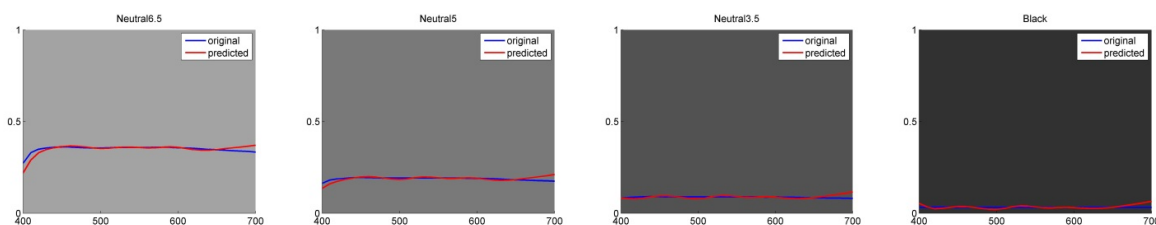


Fig.4 The original and predicted spectrum of Macbeth ColorChecker’s 24 patches

5 EXPERIMENTS AND ANALYSIS

In this section the multispectral imaging system is simulated and the proposed demosaicking algorithm is evaluated. Firstly, four wide-band Gaussian filters are set in front of the imaging sensors, and they are designed according to Eq.4 with the same bandwidth $\sigma=20$ and four distribution factors are $\mu=455\text{nm}$, 520nm , 575nm , 640nm respectively. These four filters are arranged in a 2×2 array as shown in Figure.1. The illuminant D65 is assumed and the object’s response of on the sensor can be seen as the linear transform of the illuminant spectral power. Based on the four-band MSFA the mosaicked image is generated on the single-sensor. By using the demosaicking method proposed in this paper, the other three band values of each pixel are recovered, and the corresponding spectrum information is also reconstructed by imaging system characterization. In experiment, CAVE’s hyper spectral images are employed which are treated as the capturing objects in reality, and 15 images are chosen with different objects. These images are spectrally captured from 400nm to 700nm and digitized at the resolution of 512×512 as shown in Fig.5.

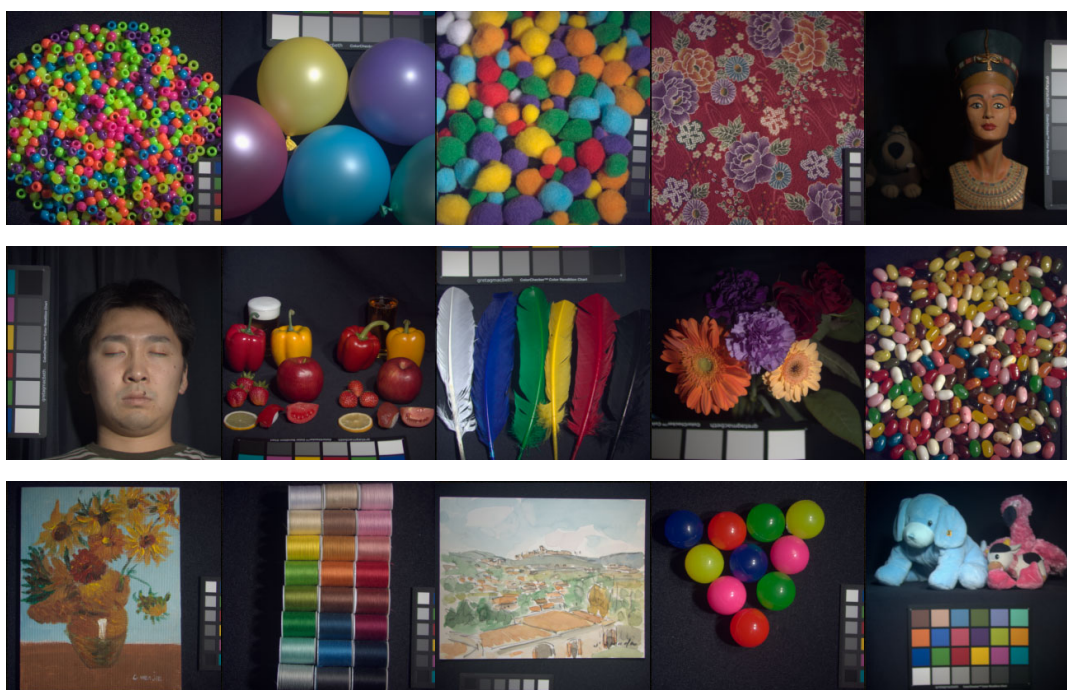


Fig.5 Fifteen hyper spectral images of CAVE

In order to evaluate the performance of the proposed multispectral demosaicking algorithm, the metrics of PSNR and RRMS are calculated from the original and demosaicked images[32,33,35]. Besides, four other demosaicking

methods are selected for comparison, they are the intra-band bilinear interpolation(defined as method-1), inter-band bilinear(method-2), binary tree-based generic method(method-3), and the demosaicking algorithm using learned interpolation weights(method-4). With different demosaicking algorithms, the recovered four-band images are compared with the original ones in PSNR values according to Eq.18, and all those fifteen testing images’ PSNR values are listed in Table.1.

Table.1 PSNR values of fifteen testing images with different demosaicking algorithms

PSNR	Method-1: Intra-band bilinear	Method-2: Inter-band bilinear	Method-3: Binary tree generic	Method-4: Weighted interpolation	Method-5: Proposed
Beads	31.3962	32.3073	30.7458	26.4825	33.2131
Balloons	44.6728	45.6692	42.0289	38.0699	46.9371
Pompoms	40.3475	41.4020	38.4598	35.0488	41.2875
Cloth	29.2961	30.8613	28.5308	24.9912	31.3640
Statue	41.8380	42.7512	40.6305	37.8052	44.1420
Face	40.0793	41.2846	38.2092	36.0451	40.2888
Food	41.7225	42.7331	40.0772	37.3722	43.2572
Feathers	35.9736	37.4261	35.1460	33.1946	39.4372
Flowers	42.1955	42.8740	39.1085	36.0687	38.4263
Beans	33.3089	35.0393	32.6284	30.6807	36.9307
Painting	31.0720	31.9940	30.8851	31.0167	34.8590
Thread	36.9233	38.6150	36.3351	37.7671	41.3007
Watercolors	32.9048	34.4912	32.2509	27.0492	36.1485
Superballs	42.5264	43.5976	41.7985	39.4690	44.9294
Toys	43.5175	43.9038	42.7080	34.5403	43.4266
Average	37.8516	38.9966	36.6361	33.7067	39.7298

Besides, the spectrum error is also calculated and compared with different demosaicking algorithms. Those fifteen images’ RRMS are listed in Table.2. The illustration of PSNR and RRMS for those images with five demosaicked algorithms is depicted in Fig.6.

Table.2 RRMS errors of fifteen testing images with different demosaicking algorithms

RRMS	Method-1: Intra-band bilinear	Method-2: Inter-band bilinear	Method-3: Binary tree generic	Method-4: Weighted interpolation	Method-5: Proposed
Beads	0.0403	0.0399	0.0407	0.0474	0.0398
Balloons	0.0160	0.0160	0.0164	0.0174	0.0160
Pompoms	0.0276	0.0273	0.0279	0.0302	0.0273
Cloth	0.0335	0.0321	0.0342	0.0408	0.0315

Statue	0.0120	0.0118	0.0121	0.0126	0.0118
Face	0.0115	0.0114	0.0118	0.0125	0.0114
Food	0.0134	0.0133	0.0137	0.0160	0.0134
Feathers	0.0224	0.0220	0.0227	0.0245	0.0218
Flowers	0.0172	0.0169	0.0176	0.0192	0.0189
Beans	0.0241	0.0233	0.0245	0.0298	0.0232
Painting	0.0208	0.0195	0.0207	0.0192	0.0163
Thread	0.0198	0.0192	0.0199	0.0194	0.0186
Watercolors	0.0229	0.0219	0.0233	0.0293	0.0212
Superballs	0.0217	0.0216	0.0217	0.0226	0.0214
Toys	0.0179	0.0178	0.0181	0.0208	0.0180
Average	0.0214	0.0209	0.0216	0.0241	0.0207

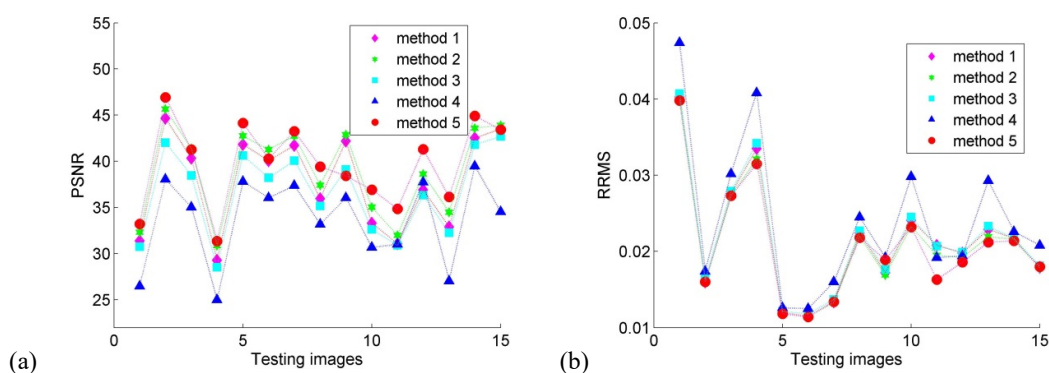


Fig.6 Comparison of different demosaicking algorithms with 15 testing images: (a)PSNR; (b)RRMS

As shown in Fig.6, our proposed method achieves the highest PSNR values and lowest RRMS errors for most of the testing images. If evaluating these five methods by the average PSNR value of the testing images, the sequence is below: $PSNR_{method5} > PSNR_{method2} > PSNR_{method1} > PSNR_{method3} > PSNR_{method4}$; similarly, the order of average RRMS is: $RRMS_{method5} < RRMS_{method2} < RRMS_{method1} < RRMS_{method3} < RRMS_{method4}$. Thus, our algorithm outperforms other models for the majority of the images. Meanwhile, because it is difficult to evaluate the demosaicking algorithms just from the objective metrics, PSNR and RRMS, the visual judgment of the reconstructed images is given for detailed evaluation. In Fig. 7, a sample of the image *feather* interpolated with different techniques is illustrated. It can be seen that less aliasing artifacts are involved in the proposed algorithm compared with other methods.

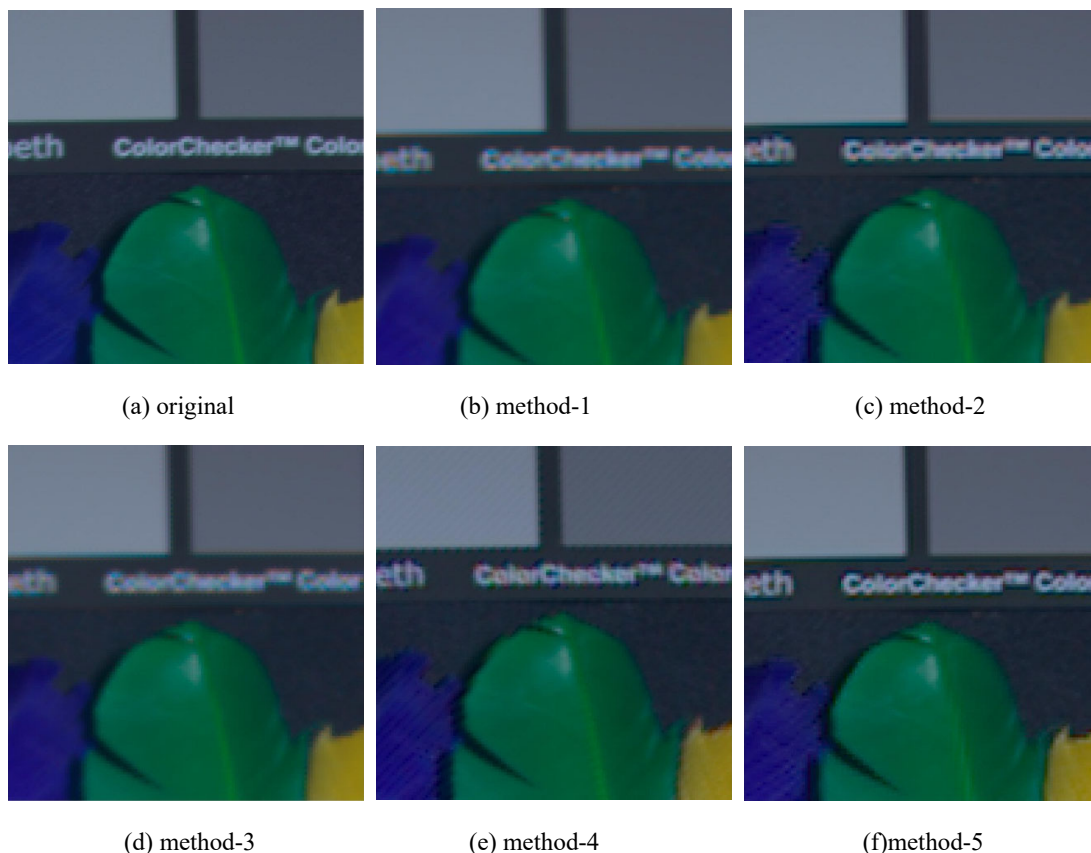


Fig.7 The original and demosaicked results of a cropped region from the image “Feathers”

6 CONCLUSIONS

The multispectral image is widely applied in the field of medicine science, environmental observation, defense and security, and other earth observation applications. For the purpose of obtaining multispectral images accurately and quickly, many solutions of multispectral cameras with single-sensor are developed in recent years. In this work, four Gaussian distributed filters are designed and arranged in a 2×2 array to create the mosaicked four-band images, and a novel demosaicking algorithm based on directional filtering and wavelet transform are proposed for the 2×2 MSFA. Within the simulation experiment, fifteen testing images are employed to evaluate different demosaicking algorithms, and the subjective assessment experiment result demonstrates less visible artifacts are involved in our proposed algorithm. Meanwhile, two objective evaluating metrics, PSNR value and RRMS error, both show the new algorithm performs better than the other four methods with most of those testing images. Thus, the experiment results indicate that the simulated four-band multispectral imaging system, especially the proposed demosaicking algorithm for 2×2 MSFA, can be applied to capture the multispectral images.

ACKNOWLEDGMENTS

The authors would like to acknowledge Shaanxi Province Key Laboratory of Printing and Packaging, Natural Science Basic Research Plan in Shaanxi Province of China (No.2017JM1028), and XUT Natural Science Foundation (No.2016CX031) for their support.

REFERENCES

- [1] Goetz, A. F. H. (2009). "Three decades of hyperspectral remote sensing of the Earth: A personal view." *Remote Sensing of Environment* 113: S5-S16.
- [2] P. Lapray, X. Wang, J. Thomas, et al. "Multispectral filter arrays: Recent advances and practical implementation," *Sensors*. 14, 21626-21659(2014).
- [3] L. Miao and H. Qi, "The design and evaluation of a generic method for generating mosaicked multispectral filter arrays," *IEEE Trans. Image Process.* 15, 2780–2791(2006).
- [4] JB Thomas, PJ Lapray, PJ, P Gouton, P, C Clerc, C. Spectral Characterization of a Prototype SFA Camera for Joint Visible and NIR Acquisition. *Sensors*. 16(7), 993 (2016).
- [5] X. Wang, J.-B. Thomas, J. Y. Hardeberg, and P. Gouton, "Median filtering in multispectral filter array demosaicking," *Proc. SPIE*, vol. 8660, pp. 86000E-1–86000E-10, Feb. 2013.
- [6] Y., Kim, K. Kim, G. Jeon, et al, "Colour interpolation using adaptive window for Bayer colour filter array." *Electronics Letters*. 50, 1689-1691(2014).
- [7] X. Chen, L. He; G. Jeon, et al. "Local adaptive directional color filter array interpolation based on inter-channel correlation." *Optics Communications*. 324, 269-276(2014):.
- [8] J. Duran and B. Antoni. "Self-Similarity and Spectral Correlation Adaptive Algorithm for Color Demosaicking." *IEEE Transactions on Image Processing*. 23, 4031-4040(2014).
- [9] Y., Monno, S., Kikuchi, M., Tanaka, et al. "A Practical One-Shot Multispectral Imaging System Using a Single Image Sensor," *IEEE TRANSACTIONS ON IMAGE PROCESSING*. 24, 3048-3059(2015).
- [10] L. Miao, H. Qi, R. Ramanath, et al, "Binary tree-based generic demosaicking algorithm for multispectral filter arrays," *IEEE Trans. Image Process.*, 15, 3550–3558(2006).
- [11] H. K. Aggarwal and A. Majumdar, "Single-sensor multi-spectral image demosaicking algorithm using learned interpolation weights," in *Proc. IEEE Int. Geosci. Remote Sens. Symp. (IGARSS)*, Jul. 2014, pp. 2011–2014.
- [12] J. Y. Kwon, M. G. Kang. Multispectral demosaicking considering out-of-focus problem for red-green-blue-near-infrared image sensors. *Journal of Electronic Imaging*. 25(2), 023010. (2016)
- [13] M. A. Martínez, E. M. Valero, J. Hernández-Andrés, et al. "Combining transverse field detectors and color filter arrays to improve multispectral imaging systems." *Applied optics* 53, C14-C24(2014).
- [14] X Wang, J B Thomas, J Y Hardeberg, et al. "Multispectral imaging: narrow or wide band filters?." *JAIC-Journal of the International Colour Association* 12 (2014).
- [15] K Parulski, "Color filters and processing alternatives for one-chip cameras." *IEEE Transactions on Electron Devices*, 32, 1381-1389(1985).
- [16] Y. Kim, J. Jeong. Four-Direction Residual Interpolation for Demosaicking *IEEE Transactions on Circuits and Systems for Video Technology*. 26(5) : 881-890. (2016)
- [17] D. Menon and C. Giancarlo, "Color image demosaicking: an overview." *Signal Processing: Image Communication* 26, 518-533(2011).
- [18] B. G. Jeong, S. H. Hyun, and I. K. Eom, "Edge adaptive demosaicking in wavelet domain," in *Proceedings of the 9th International Conference on Signal Processing (ICSP'08)*, pp. 836–839, Beijing, China, October 2008.
- [19] D. Sung, H. Tsao. Color Filter Array Demosaicking by Using Subband Synthesis Scheme. *IEEE SENSORS JOURNAL*. 15(11):

6164-6172. (2015).

- [20] Y. Kim, K. Kim, G. Jeon et al.. "Colour interpolation using adaptive window for Bayer colour filter array." *Electronics Letters* 50, 1689-1691(2014).
- [21] D Menon, S Andriani, G Calvagno. "Demosaicing with directional filtering and a posteriori decision." *IEEE Transactions on Image Processing*, 16, 132-141(2007).
- [22] L Shao and A U Rehman. "Image demosaicing using content and colour-correlation analysis." *Signal Processing* 103 (2014): 84-91.
- [23] H S Kim, S S Kim, I K Eom. "Wavelet-domain demosaicking using linear estimation of interchannel correlation." *Optical Engineering* 47, 067002-067002(2008).
- [24] X. Jia, B. Zhao, M. Zhou et al. "An edge-adaptive demosaicking method based on image correlation." *Journal of Central South University*, 22, 1397-1404(2015).
- [25] S. Susan, D. Aneja. Edge Strength based Fuzzification of Colour Demosaicking Algorithms. *Defence Science Journal*. 64(1): 48-54. (2014).
- [26] C. A. Laroche and M. A. Prescott, "Apparatus and method for adaptively interpolating a full color image utilizing chrominance gradients," U.S. Patent 5,373,322, 1994.
- [27] J. E. Adams and J. F. Hamilton, "Design of practical color filter array interpolation algorithms for digital cameras," in *Proc. SPIE*, vol. 3028, 1997, pp. 117–125.
- [28] D. Alleysson, S. Susstrunk, and J. Herault, "Color demosaicing by estimating luminance and opponent chromatic signals in the fourier domain," in *Proc. Color Imaging Conference: Color Science, Systems, and Applications*, 2002, pp. 331–336
- [29] N Lian, L Chang, Y P Tan, "Improved color filter array demosaicking by accurate luminance estimation." *Image Processing*, 2005. *ICIP 2005. IEEE International Conference on*. Vol. 1. IEEE, 2005.
- [30] L Chen, KH Yap, Y He. "Subband synthesis for color filter array demosaicking." *IEEE Transactions on Systems, Man and Cybernetics, Part A: Systems and Humans*, 38,485-492(2008).
- [31] J Driesen, and P Scheunders. "Wavelet-based color filter array demosaicking." *Image Processing*, 2004. *ICIP'04. 2004 International Conference on*. Vol. 5, pp. 3311-3314. IEEE, 2004.
- [32] R Niruban, T S R Raja, and T S Sharmila. "novel color filter array demosaicing in frequency domain with spatial refinement." *Journal of Computer Science* 10, 1591(2014).
- [33] B Sun, H Liu, S Zhou, et al. "Modified Spectral Neugebauer Model for Printer Characterization." *Spectroscopy Letters*. 48, 660-668(2015).
- [34] B Sun, H Liu, S Zhou, et al. "Evaluating the Performance of Polynomial Regression Method with Different Parameters during Color Characterization." *Mathematical Problems in Engineering* 2014, 418651 (2014).
- [35] L. S. Chow, H. Rajagopal, R. Paramesran. Correlation between subjective and objective assessment of magnetic resonance (MR) images. *MAGNETIC RESONANCE IMAGING*. 34(6): 820-831. (2016)